Available online at www.sciencedirect.com
SCIENCE DIRECT®
Journal of Nuclear Materials 328 (2004) 1–10
journal of nuclear materials
www.elsevier.com/locate/jnucmat

Deformation of zirconium irradiated by 4.4 MeV protons at 347 K

C.K. Chow [a], R.A. Holt [b,*], C.H. Woo [c], C.B. So [d]

[a] AECL, 2251 Speakman Drive, Mississauga, ON 15K 1B2, Canada
[b] Department of Mechanical Engineering, Queen's University, McLaughlin Hall, Stuart Street, Kingston, ON K7L 3N6, Canada
[c] Hong Kong Polytechnical University, Hung Hom, Hong Kong SAR, China
[d] Nuclear Safety Solutions Inc., 700 University Avenue, Toronto, ON M5G 1X6, Canada

Received 7 February 2003; accepted 21 January 2004

Abstract

Proton irradiation tests have been performed on two cold-worked zirconium specimens using 4.4 MeV protons with controlled displacement damage rates between 1.4 and 6.9×10^{-7} dpa s^{-1}. The specimens had different Fe contents, nominally pure (NP): 64–70 ppm by weight, and ultra-high purity (UP): 3–5 ppm by weight. A stress of 50 MPa was applied during the tests, and the test temperature was 347 K.

1. Introduction

Irradiation growth of zirconium alloys has now been extensively studied both experimentally and theoretically. The salient characteristics of the long term growth rate of Zr alloy polycrystals are (i) expansion along directions containing a high proportion of *a*-axes, (ii) contraction along directions containing a high proportion of *c*-axes, (iii) an increase in the early growth rate with increasing density of the original dislocation network, (iv) the growth rate in materials with a low initial network dislocation density increases with fluence as the population of *c*-component defects (dislocations/loops) grows, and (v) the growth rate is linear in displacement damage rate at temperatures down to 330 K. There seems to be a consensus that at high temperatures (where vacancies are mobile) growth can be accounted for using a combination of:

(a) The traditional rate theory description of growth and swelling where the point defects react with sinks in proportion to 'sink strength' and a bias due to interaction of self-interstitial atoms (SIAs) with dislocation strain fields [1], but where the bias is due to is the 'diffusional anisotropy difference' (DAD) between vacancies and SIAs as proposed by Woo et al. [2,3]. This theory seems to adequately explain growth at 'normal reactor operating temperatures' (470–620 K).

(b) The 'production bias' theory developed by Woo and co-workers [4,5], in which different proportions of vacancy and interstitial 'primary clusters' are formed in the cascades caused by neutron damage and these clusters are immobile, and therefore are only accessible to mobile sinks (dislocations via climb and glide). This theory appears to adequately explain the strong temperature dependence of growth at higher temperatures, associating that with the 'evaporation' of the primary vacancy clusters. The theory has been further expanded to allow for the stochastic nature of cascade events in both time and space. This gives mobile sinks (network dislocations, loops) an effective 'diffusivity' that allows them to interact with immobile defects whether or not they exhibit a net 'drift' [6,7].

Growth at lower temperatures is a different matter. Early results for cold-worked material irradiated at 330–350 K demonstrates the same shrinkage along directions containing a high proportion *c*-axes as at high

* Corresponding author.
E-mail address: holt@me.queensu.ca (R.A. Holt).

0022-3115/$ - see front matter Crown Copyright © 2004 Published by Elsevier B.V. All rights reserved.
doi:10.1016/j.jnucmat.2004.01.017

temperatures [8] showing that true growth is occurring (at approximately constant volume), by precipitation of SIAs on the prism planes and vacancies on the basal planes. The fact that the growth rate does not saturate in cold-worked materials as it does in annealed materials shows that the network dislocations are acting as sinks for the point defects, which would otherwise recombine. Subsequent data at 330 K indicated that, as at higher temperatures, the steady state growth rate is linearly proportional to the displacement damage rate [9]. In annealed material the growth quickly saturates (unless there are significant built-in intergranular constraints between different crystal orientations due to cold-worked, or annealing [10]) and no further change in dimensions occurs (to fluences up many 10s of displacements per atom (dpa)).

In annealed material, the *a*-loop structure is barely visible by TEM (loops <5 nm). X-ray line broadening indicates saturation in the dislocation density after about 5 dpa. No *c*-component loops form in annealed material to fluences equivalent to ~40 dpa. Typically, the *a*-loop structure in cold-worked material irradiated at 330 K is similar to that in annealed material, i.e., a high density of sub-5 nm loops, which appears to saturate quickly. Cold-worked material also contains network *a* and $c + a$ dislocations. It is apparent that, during growth, the $c + a$ dislocations are acting as net vacancy sinks (to give a negative strain along the *c*-axis), while the *a*-loops and network dislocations act as net SIA sinks.

The major issue in explaining the growth in cold-worked material in this temperature range (330–350 K) is the detail of the arrival of the vacancies at sinks. This has been the subject of numerous model calculations. With the rate theory/DAD formulation for growth, the sensitivity of the growth rate to displacement damage rate depends upon whether the point defect kinetics are 'sink controlled' or 'recombination controlled'. In the former case, the growth rate is linearly dependent on the displacement damage rate, while in the latter case the growth rate is proportional to the square route of damage rate. The transition from sink-controlled behaviour to recombination-controlled behaviour depends upon the vacancy mobility. Early attempts to model growth at low temperatures [9,11] assumed 'facile' vacancy migration to be occurring in zirconium, with a much lower activation energy than would be expected based on melting point, and atomic size considerations [12]. Hood and co-workers [13,14] subsequently showed that the observations of low self-diffusion activation energies (previously attributed to 'facile' vacancy migration) are an extrinsic affect associated with the presence, in solution, of Fe, which is hypothesized to form a fast diffusing binary complex with the vacancy [15]. Superficially, this effect would be expected to be infinitesimal at 330–350 K because of the low solubility of Fe [7]. However irradiation is known to redistribute iron [16] and it is possible that Fe solubility is enhanced under irradiation and this could explain the apparent mobility of vacancies in the HVEM [17].

In this paper, we describe an experiment designed to test whether the concentration of Fe at relatively low levels affects the growth characteristics of Zr. Proton irradiation is ideally suited to this purpose because the beam current can be controlled to assess the dependence of the growth rate upon the displacement damage rate, i.e., the value of the damage rate exponent, *n*, in the expression

$$\dot{\varepsilon} \propto K^n, \tag{1}$$

where $\dot{\varepsilon}$ is the growth rate and K is the displacement damage rate, can be readily determined. The tests results of proton irradiation of two pure zirconium specimens with different Fe contents are reported.

2. Experimental details

2.1. Materials

The initial material was nominally pure (NP) Zr with about 60 ppm (by wt) of Fe. Some of this material was further purified by electro-transport and the Fe content was reduced to about 5 ppm (by wt). This is referred to as ultra-high purity (UP) material. These materials were cold rolled into foils as follows.

For proton transparency, the specimen has to be less than 50 μm thick. This was achieved by steps of 50% cold rolling, followed by vacuum ($<10^{-7}$ Pa) annealing at 500 °C for 1 h. Initially the material was rolled between Zr sheets to reduce the Fe contamination by the steel rollers. However, the material developed a cup shape due to differential deformation of the covering Zr sheet and the core material and this technique was abandoned. During subsequent reductions, the materials were rolled between steel rollers. It was found that the Fe contamination was restricted to a surface layer 0.5 μm thick, and that this layer could be easily removed by chemical polishing before vacuum annealing. This procedure was repeated until a thickness of 120 μm was reached. The final 50% cold roll was followed by a stress relieve at 120 °C for 2 h in Ar. For this final heat treatment, the specimen was rapped in zirconium foil to reduce oxidation. The specimen remained shiny after the heat treatment indicating insignificant oxidation. Dog-bone shaped specimens with gauge length 25 mm long by 4 mm wide were punched from the foils. The specimens were then chemically polished (45%H_2O, 45%HNO_3, 5%HF) to remove any surface contamination and reduced to the thickness to about 50 μm thick before mounting in the test rig.

X-ray diffraction was performed on foils to determine the texture and dislocation densities. Transmission electron microscopy was used to determine the grain size. The Fe contents of the materials were analyzed using secondary ion mass spectrometry (SIMS) before and after the tests.

2.2. Experimental setup

The test rig, Fig. 1, was enclosed in a temperature controlled chamber filled with He. The temperature of the chamber was controlled at 278 K by four heat exchangers supplied by constant temperature water circulation. Fans were installed behind the heat exchangers to enhance the circulation. The ends of the specimens were clamped with Invar grips with the gauge length open to the proton beam on one side and to line-of-sight of a fast responding radiometer (Barnes Engineering, Model RM2A) on the other. A fan directed the helium to cool the specimen so that a high intensity proton beam could be used.

A stress of 50 MPa was applied to the specimen by dead load to keep the specimen straight and obtain accurate strain measurements. The elongation of the specimen was measured by an LVDT affixed to the stationary lower grip by an Invar bar, and mounted on the same axis as the specimen measuring the displacement of the moving upper grip.

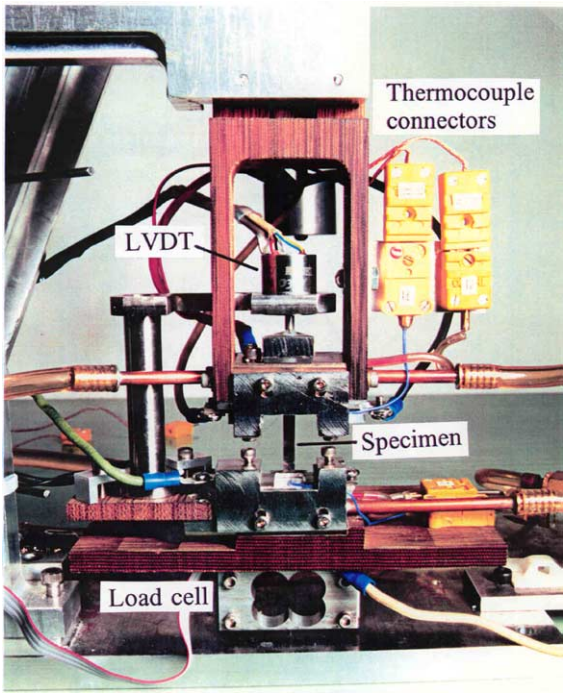

Fig. 1. Experimental apparatus.

The proton beam of approximately 1 mm diameter was rastered by two sets of magnetic coils with frequencies 1200 Hz in the vertical and 100 Hz in the horizontal directions. The proton beam ionized the helium gas and the beam could thus be seen to centre it on the specimen.

2.3. Test temperature

The temperature of the test specimen was monitored by the infrared radiometer, calibrated using blackbodies. The temperature of the specimen was deduced from this calibration curve after correction for the emissivity. The emissivity of the specimen before and after each test was measured and found to remain constant at 0.16 although the specimen had a slight blue coloration after testing. This was consistent with a previous finding that slight discoloration will not affect the emissivity of zirconium alloys [18]. The emissivity of electro-polished zirconium exposed to air at 80 °C was measured and it was found to be 0.15, agreeing with the previous work. No change was observed for 2000 h.

The radiometer was placed inside the experimental chamber so that the infrared signal did not have to go through a window. To correct for the possible drift of the radiometer, a reference signal was obtained from an NP Zr foil kept at the test temperature. This foil was clamped on a heater, the temperature of which was measured and controlled by thermocouples. The stability of the temperature of the heater was better than 0.5 °C. The surface temperature of this reference foil was measured by attaching a fine gauge thermocouple to it and found to be identical to the heater temperature. This heater assembly was placed inside the test chamber so that it was exposed to the same atmosphere as the specimen under irradiation to ensure that if there was a change in emissivity due to reaction with the environment, the specimen and the reference foil would change in the same manner. During irradiation, the radiometer monitored the temperature of the specimen. When irradiation is stopped, the radiometer was calibrated using the reference. It was found that the drift of the radiometer was less than 1 °C.

The specimen temperature was controlled by passing a direct current through the specimen to maintain a constant infrared signal. The system response was fast enough to compensate for variations in heating of the specimen by the proton beam. An electronic controller with proportional, integral and differential modes (PID controller) was built for this purpose.

The InSb sensor of the radiometer requires cooling to liquid nitrogen temperature. When the liquid nitrogen reservoir was refilled, the radiometer interior temperature dropped. As the radiometer took the reference temperature from the signal chopper in the interior chamber, the output signal increased. The temperature

controller, in maintaining the radiometer signal constant, would reduce the specimen temperature to compensate. At the beginning of the test, the specimen temperature drop was about 2.3 °C, deduced from the length change of the specimen and the thermal expansion coefficient of the Zr. Later on, this effect was reduced by more frequent liquid nitrogen filling and the specimen temperature drop was reduced to about 0.8 °C. As the irradiation deformation is relatively insensitive to temperature in the range of interest [19], this temperature swing was not expected to affect the results.

The influence of the glow from the ionized helium on the temperature measurement was tested by turning the proton beam on and off without the specimen. There was no effect on the radiometer reading.

2.4. Strain measurement

The strain measurement during the test was performed by a Pickering DC-DC LVDT, model 7304, with specified resolution and repeatability of better than 2.5×10^{-2} μm. The deviation from linearity was 0.1%. The temperature coefficient of the LVDT was a function of the output (core location) and it was found that it is minimum when the output is 150 mV. Therefore, the LVDT was adjusted so that the output was close to 150 mV before the test started. To further reduce the effect of temperature, the LVDT was kept at constant temperature (20.0 ± 0.1 °C) by a water jacket. Because of the specimen temperature fluctuation during the test due to the liquid nitrogen filling, the strain was measured with the proton beam and the DC heating turned off. The temperature of the specimen would drop to the chamber temperature. The LVDT reading indicated that the temperature would settle in about 10 min and after which time the LVDT reading would change by less than 0.2 mV (corresponds to a strain of about 5×10^{6}). The reading was made after 20–30 min.

2.5. Proton dose

The irradiation was performed with protons of energy 4.4 MeV. With this energy, most of the protons pass through the specimen, minimizing hydrogen deposition, and creating a fairly uniform displacement damage profile [20]. The dose in the specimen was estimated from the power generated in the specimen by the proton beam. The power required to maintain the specimen at the test temperature with no proton beam was noted before the test and during the test for short periods of time (e.g., during accelerator trips). With the proton beam on the specimen, the power required to maintain the specimen at the test temperature is reduced and the difference in power was used to calculate the proton beam intensity. The displacement damage rate was calculated using the NRT model assuming a threshold displacement energy for zirconium of 25 eV. The uncertainty in the mean power requirement with no proton beam was usually about ±2% and rarely varied more than 4% between measurements. The dose was calculated numerically by summing the product of displacement rate and time and the maximum error was estimated as about 10%. The displacement rate in these tests was controlled between 1.4 and 6.9×10^{-7} dpa s^{-1} by controlling the beam current.

2.6. Fe concentration measurement

The concentration of Fe was measured by secondary ion mass spectrometry (SIMS) at CANMET (Canada centre for Mineral and Energy Technology in Ottawa Ontario). It is believed that this technique is more accurate than other available methods for measuring low Fe concentrations in Zr [14].

3. Results

3.1. Fe concentrations

Before the test, the bulk Fe contents of the specimens were 64 and 5 ppm by wt for the NP and the UP specimens, respectively. After the test, higher Fe concentrations were found on the surfaces of the UP specimen. In the bulk, the Fe content was about 72 ppm in the NP specimen and 3 ppm in UP specimen. The value of 3 ppm was measured at about 12 μm below the surface. At 2.5 μm below the surface, the Fe concentration was 14 ppm. The source of surface Fe is not clear but could be atoms sputtered from the Invar grips or the result of irradiation-induced migration of Fe to the surface.

3.2. Microstructure of the specimens

The texture was measured and the dislocation density estimated using X-ray diffraction [21,22]. The inverse pole figure in the normal direction of the foil indicated that the resolved fraction of basal plane normals in the foil normal direction was, typically, 0.74. The *a*-type dislocation density was estimated to be 0.97×10^{14} m^{-2}.

Grain size measurements were carried out using TEM. Because of the heavy deformation and the sharp texture, the grain boundaries were not clearly defined. About 20 grains were randomly chosen from the thin regions and the size estimated. The result showed that the grains were about 2 ± 1 μm long (rolling direction) and 0.4 ± 0.2 μm wide the plane of the foil. However, because of the difficulty in clearly defining the grain boundaries, this is only a rough estimate. Based on the geometry of the rolling strains it is likely that the dimension of the grains normal to the foil is even finer.

3.3. Strain rates and their dose rate dependence

The damage rate histories of the specimens, and the corresponding cumulative strains are shown in Tables 1 and 2. The strains of the specimens are shown as a function of time in Figs. 2 and 3. There was some exposure to the NP specimen during set-up, and an unknown amount of strain was accumulated before the

Table 1
Damage rate details for NP specimen

Elapsed time (h)	Damage rate (dpa $s^{-1} \times 10^7$)	Cumulated strain (%)
20.3	Set-up	0.000
30.3	5.4	0.024
72.8	2.0	0.035
96.3	6.9	0.054
127.8	3.6	0.069
143.8	5.2	0.079
148.8	6.9	0.082
174.8	1.9	0.088

Table 2
Damage rate details for UP specimen

Elapsed time (h)	Damage rate (dpa $s^{-1} \times 10^7$)	Cumulated strain (%)
15.8	2.2	0.011
39.0	5.8	0.034
60.9	2.6	0.041
81.3	5.9	0.059
103.1	4.4	0.072
129.4	1.8	0.078
149.4	6.1	0.095
168.6	2.4	0.099
190.6	4.4	0.109
216.4	1.4	0.112
256.4	6.2	0.144
274.9	3.1	0.150
321.9	6.2	0.185
348.3	3.4	0.197
366.9	6.2	0.209

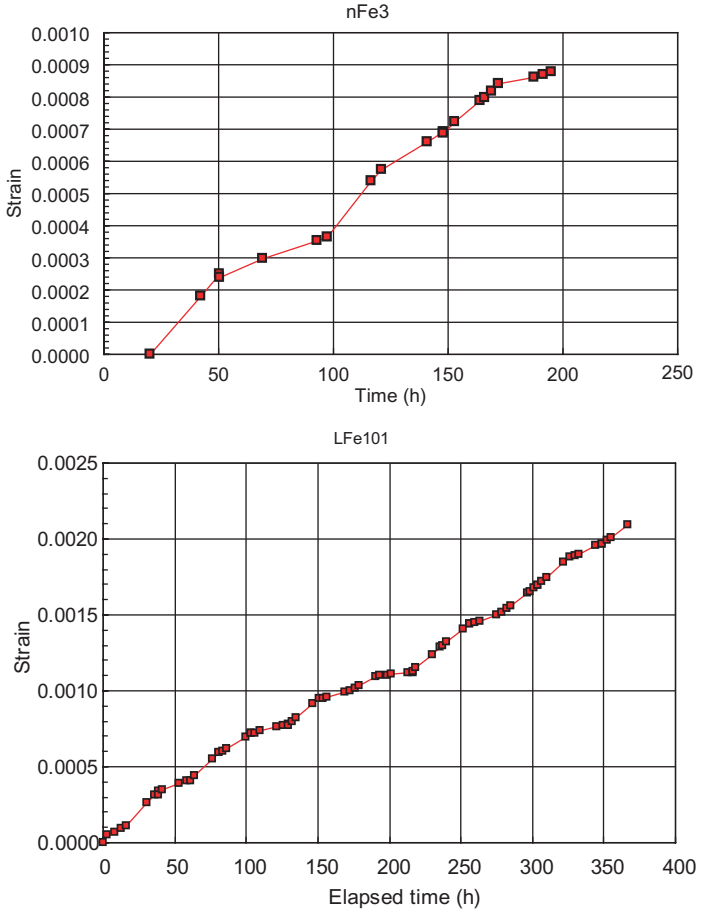

Fig. 2. Irradiation deformation of the specimens as a function of time. The change of slopes was due to the change of dose rates.

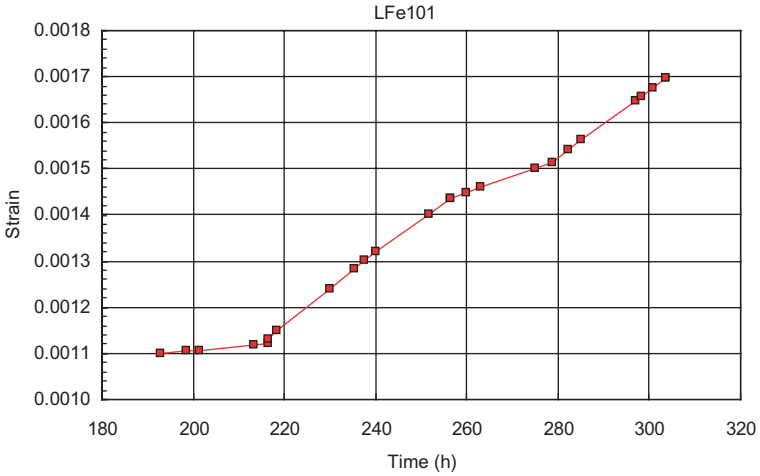

Fig. 3. Details of the strain–time plot. Note that there is little transient after the dose rate change.

strain measurements started. In both cases the specimens ceased to deform if the proton beam was interrupted, consistent with Faulkner and McElroy's finding [23]. Fig. 3 gives a detail of Fig. 2, showing that there was little transient due to the change of dose rate, consistent with results by Chapman et al. [20] in their studies on irradiation creep and growth of Zircaloy-2 under proton irradiation.

Fig. 4 shows the strain as a function of dose for both specimens. The smooth curve indicates that the strain rate is close to a linear function of the dose rate. The strain rate is plotted as a function of dose in Fig. 5. After about 0.1 dpa, the strain rate leveled off at $3.3 \pm 0.5 \times 10^{-3}$ dpa^{-1} (UP material) and $3.2 \pm 0.2 \times 10^{-3}$ dpa^{-1} (NP material).

Assuming that the strain rate is related to the dose rate according to a power law with exponent n, Eq. (1), n can be determined from adjacent dose rate. The results are plotted in Fig. 6. The first point from the UP specimen LF101 should be discarded because it was calculated from points at which the deformation was undergoing a transient. Once the deformation was beyond the transient (>0.1 dpa), the exponent n was close to 1 for both cases. The average of the exponent for the NP and UP specimens are 1.12 ± 0.14 and 1.15 ± 0.17, respectively.

4. Discussion

The total strain rates observed here are slightly more than 3×10^{-3} dpa^{-1}. Because there was a load of 50 MPa on the specimens, this strain comprises both creep and growth components. In these tests, only one load was used and it is impossible to separate the growth and creep strains. If the strain rate were entirely due to growth, approximately 1% of the point defects are contributing to the strain. Rogerson [24] reported that the growth rates for 18% swaged zirconium crystals irradiated by neutrons at 80 °C was $\sim 1.3 \times 10^{-28}$ m^2 n^{-1}, which is equivalent to 5×10^{-4} dpa^{-1}, about 15% of our total strain rate. This disagreement could be due to one or more of the following: the difference between the efficiencies of the cascade and Frenkel pair damage, a major contribution of creep to the strain in the proton case, and the very fine grain size of the sample in the proton case, the grain boundaries providing additional sinks for point defects (it should be noted that this fine grain size is typical of some zirconium alloys). In any case, the near linear damage rate dependence of the strain rate (our tests show that for both materials, n of Eq. (1) is ~ 1.1) must be explained (the same arguments with respect to dose-rate dependence and vacancy mobility apply to both irradiation growth and irradiation creep).

This could mean either that the amount of Fe in the UP material was enough to induce fast diffusion, or that the conventional theory is not adequate to explain the observation. Woo [7] included the effect of iron-vacancy pair formation in his rate theory formulation of irradiation damage in Zr. The pursuant analysis showed that the concentration of the fast diffusing iron-vacancy pair depends on the solid solubility of iron in α-Zr. Under thermodynamic equilibrium conditions, this is extremely low (<0.1 μm). Radiation-induced dissolution causes a local solute supersaturation near the second phase, some of which diffuse outwards down the concentration gradient. The iron solute atoms that enter into the α-matrix may react with the vacancies to form fast diffusing pairs, but they may also react with various sinks and traps (such as other alloying elements) or may re-precipitate. Due to the extremely low solid solubility of iron in the α-matrix, unless the local concentration near the dis-

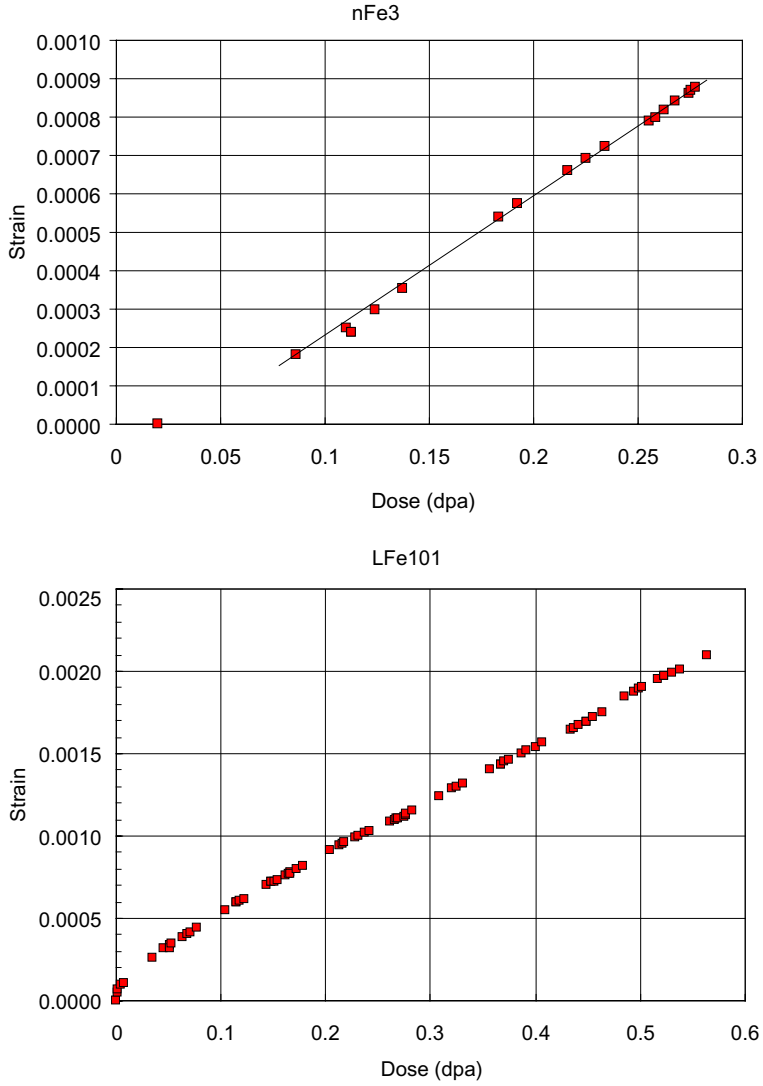

Fig. 4. Strain as a function of dose. The smooth curve indicates that the strain rate is only a weak function of the dose rate.

solving precipitate is sufficiently low, most of the iron dissolved during irradiation may re-precipitate in small submicroscopic particles formed during irradiation. Thus, the dissolution of iron does not necessarily mean that a supersaturation of iron solute can be maintained at a level sufficiently higher than the equilibrium concentration that significant reactions with sinks, traps and vacancies occur during irradiation. Based on this reasoning, Woo [7] concluded that below 400 °C, there would be no noticeable effect of Fe in Zr alloys in the temperature range of these experiments. Our results agree with his assessment.

The total strain in the material with 5 ppm Fe during the experiment was >0.002. Even assuming that growth is 100% efficient (all of the vacancies deposited at sinks actually causing measurable strain) each Fe atom would have to account for the transport of >250 vacancies to sinks in order to explain the linear growth rate sensitivity. During the experiment each Fe atom would have to travel about half the mean distance between sinks ($\sim 5\times10^{-8}$ m) 250 times during the duration of the experiment (1.32×10^{6} s). This corresponds to a diffusion coefficient of 4.7×10^{-19} m^2s^{-1}, 8–9 orders of magnitude faster than expected, based on extrapolation of high temperature data for diffusion of Fe in Zr [14]. It is therefore unlikely that the conventional rate theory is adequate.

The conventional theory assumes that the damage occurs in the forms of freely migrating vacancies and SIAs, homogeneously in space and uniformly in time.

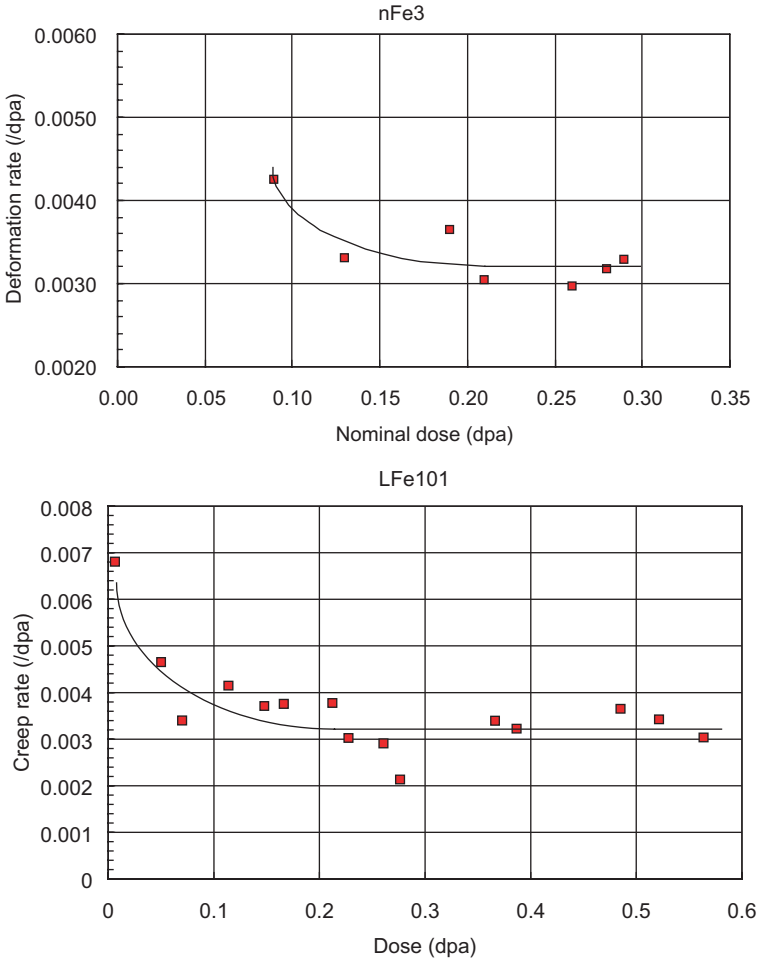

Fig. 5. Strain rate as a function of dose.

The SIAs have high diffusivity even at low temperatures. When the vacancies have high diffusivity they can diffuse to sinks, and the vacancy concentration stays low, so there is little direct recombination of vacancies and SIAs. When the vacancy diffusivity is low (or the damage rate is high), their concentration builds up, and more direct recombination takes place, reducing the growth rate, and reducing its sensitivity to displacement damage rate. At still lower temperatures (or higher displacement damage rates) the vacancies are effectively frozen in the lattice and all recombine, causing the growth rate to effectively stop. At the conditions of this experiment, the vacancy mobility is low relative to the time scale. Using a typical activation energy expected for vacancy migration in Zr (1.4 eV) a vacancy being expected to move <2 lattice spacings over the duration of the experiment.

During irradiation by neutrons and heavy ions, however, interstitial and vacancy clusters are formed and removed at different rates. Production bias theory [4,5] was developed to take into account the formation and lifetime of vacancy and interstitial clusters in the cascades. Subsequently the stochastic nature of the temporal variation in point defect fluxes was incorporated into the model [6]. An important feature of the production bias/stochastic theory is that the dislocation segments also have an effective diffusivity, which originates from the stochastic nature of point-defect arrival at the sinks. Even at low temperatures where vacancies are effectively immobile, dislocations climb due to interstitial absorption and glide due to the evolving stresses in the structure. With proton irradiation the majority of the point defects are generated as Frenkel pairs, with a few larger cascades, but even with Frenkel pair generation, the process is stochastic in nature and climb is expected to occur in bursts. This allows dislocation lines to glide and 'sweep-up' some of the relatively immobile vacancies [6].

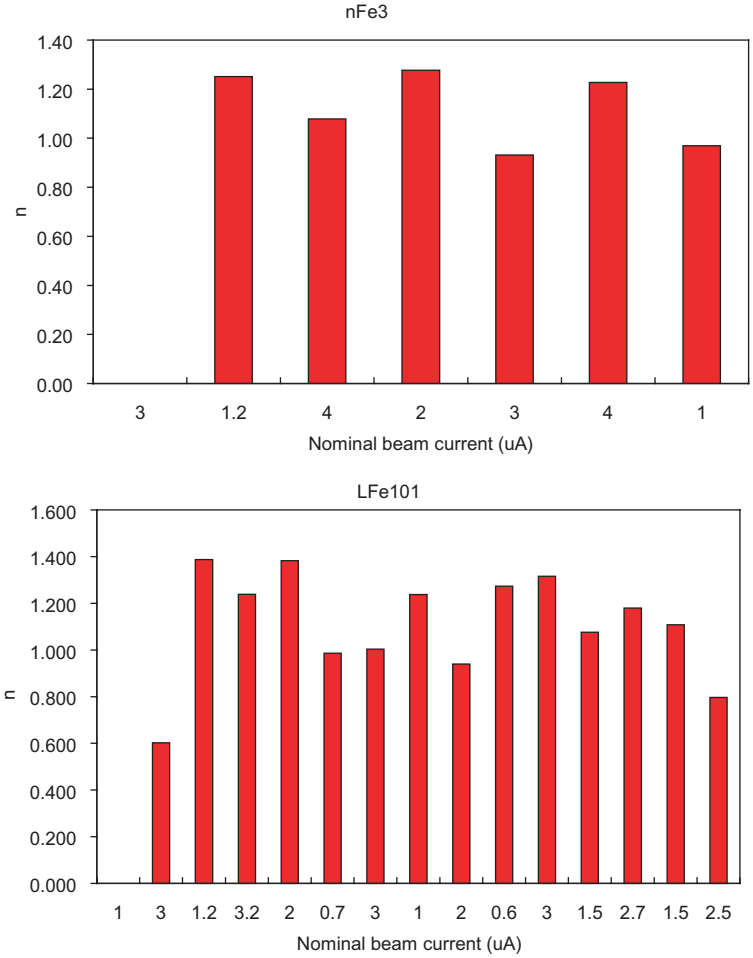

Fig. 6. Exponent n as a function of beam current (a) for NP specimen NF3 (b) for UP specimen LF101.

Woo [7] was able to replicate most of the low temperature observations with a combination of the DAD driven rate theory and the production bias theory. Vacancies are immobile, but are annihilated at dislocation sinks that are mobile. Although the predicted growth rates agree with experiment, the displacement damage rate dependence was not examined in detail. Nevertheless, as shown by Woo [7] the quantity η that governs the long-range recombination of vacancies and SIAs can be written as

$$\eta = \frac{4\alpha G}{D_i(D_v + D_d)k_i^2 k_v^2}, \tag{2}$$

where k_j^2 are the total sink strengths, and D_j, the diffusivities, for SIAs $(j = i)$ and vacancies $(j = v)$, respectively. α is long-range recombination coefficient, and G is the effective dpa rate. The thermal component D_d is the effective diffusivity of the dislocation segments due to their drift and stochastic motion and may be related to the dislocation-cluster interaction constant W in the production bias theory [6] by $ZD_d = W$. The value of η does not diverge, even when D_v vanishes (i.e., practically) at low temperatures. Using a value of W as in [5], the condition $\eta \ll 1$ is satisfied for a sink strength of 10^{16} m^{-2}. This sink strength, although high, is the typical sink strength one normally encounters under cascade irradiation conditions such as due to neutron damage, resulting from the accumulation of immobile interstitial clusters [6]. This would result in a linear dose rate dependence in the deformation rate.

Motta et al. [25] have recently examined the possibility that sufficient vacancies could be directly deposited on existing sinks in the microstructure during displacement events to account for the growth stain rate observed, concluding that such a mechanism is just possible for the case of neutron irradiation. Again the case of proton irradiation was not examined.

Finally, one must consider the possibility that, despite evidence to the contrary [14] vacancies exhibit

some intrinsically fast mode of migration at low temperatures.

Clearly more work is needed to fully explain the current results.

5. Summary and conclusions

Proton irradiation tests have been performed on two cold-worked Zr specimens using 4.4 MeV protons with displacement damage rates of 1.4 to 6.2×10^{-7} dpa s^{-1}. The specimens had different Fe contents – nominally pure (NP) and ultra-high purity (UP). Fe analysis by SIMS showed that the UP specimen contained in the bulk about 5 ppm by wt Fe before irradiation and about 3 ppm after irradiation and the NP specimen contained in the bulk about 64 ppm before and 70 ppm Fe irradiation. A stress of 50 MPa was applied during the tests, and the test temperature was 74 °C.

The following conclusions are drawn:

- The observed deformation rates were entirely due to irradiation. Deformation stopped when the proton beam was turned off.
- The dose rate exponents n were 1.12 ± 0.14 and 1.15 ± 0.17 for the UP and NP materials, respectively, i.e., not significantly different from 1 or from each other. The strain rate could therefore be expressed in units of dpa^{-1}.
- After the initial transient, there was no difference in the rate of deformation between the UP and the NP material. After about 0.1 dpa, the deformations rate of both materials remains constant at about 3.2×10^{-3} dpa^{-1}.
- Under the conditions of the irradiation, in the concentration range 3–70 ppm Fe by wt, Fe has no effect on the radiation-induced deformation rate of zirconium.
- The linear damage rate dependence observed cannot be explained by extrinsic facile vacancy migration due to the presence of Fe.

Acknowledgements

The experimental work reported here was undertaken while the authors were members of Reactor Materials Research Branch, AECL and was funded by the CANDU Owners Group, Working Party 32. Subsequent work was funded by the National Sciences and Engineering Research Council of Canada, Ontario Power Generation Inc., the CANDU Owners Group Inc. and the Research Grant Council of HKSAR (Grants#PolyU5177/02E and PolyU5167/01E). The authors thank T. Riemer, S. Hosein, J. Roy, H. Zou, K. Demoline, J. Mecke, J. Winegar, R. Styles and L. Lauren for contributions to this work. The materials were kindly supplied by G. Hood, and the manuscript was edited by M.J. Kingston.

References

[1] A.D Brailsford, R. Bullough, J. Nucl. Mater. 44 (1972) 121.
[2] C.H. Woo, U.M Gosele, J. Nucl. Mater. 119 (1983) 219.
[3] C.H. Woo, J. Nucl. Mater. 159 (1988) 237.
[4] C.H. Woo, B.N. Singh, Philos. Mag. A 65 (1992) 889.
[5] R.A. Holt, C.H. Woo, C.K. Chow, J. Nucl. Mater. 205 (1993) 293.
[6] A.A. Semenov, C.H. Woo, J. Appl. Phys. A 67 (1998) 193.
[7] C.H. Woo, Radiat. Eff. Def. Solids 144 (1998) 145.
[8] R.A. Murgatroyd, A. Rogerson, J. Nucl. Mater. 90 (1980) 240.
[9] R.A. Holt, J. Nucl. Mater. 159 (1988) 310.
[10] A.R. Causey, C.H. Woo, R.A. Holt, J. Nucl. Mater. 159 (1988) 225.
[11] R. Bullough, M.R. Haynes, M.H. Wood, J. Nucl. Mater. 90 (1980) 44.
[12] G.M. Hood, J. Nucl. Mater. 159 (1988) 149.
[13] G.M. Hood, H. Zou, D. Gupta, R.J. Schultz, J. Nucl. Mater. 233 (1995) 122.
[14] H. Zou, G.M. Hood, R.J. Schultz, J.A. Jackman, J. Nucl. Mater. 210 (1994) 239.
[15] A.D. King, G.M. Hood, R.A. Holt, J. Nucl. Mater. 185 (1991) 1045.
[16] M. Griffiths, J. Nucl. Mater. 205 (1993) 225.
[17] M. Griffiths, R.C. Styles, C.H. Woo, F. Phillipp, W. Frank, J. Nucl. Mater. 208 (1994) 324.
[18] E.V. Murphy, F.J. Havelock, J. Nucl. Mater. 60 (1976) 167.
[19] R.A. Holt, A.R. Causey, V. Fidleris, in: Dimensional Stability in Irradiated Metals and Alloys, 1, BNES, London, 1983, p. 175.
[20] O.J.V. Chapman, R.J. McElroy, B.E. Sheldon, in: Proceedings of the 6th International Symposium on Zirconium in the Nuclear Industry, ASTM STM 824, 1984, p. 343.
[21] J.E. Winegar, Atomic Energy of Canada, Report AECL 5626, 1977.
[22] M. Griffiths, J.E. Winegar, J.F. Mecke, R.A. Holt, Adv. X-ray Anal. 35 (1992) 593.
[23] D. Faulkner, R.J. McElroy, in: Effects of Irradiation on Materials: Proceedings of the 9th International Symposium, ASTM STP 683, 1979, p. 343.
[24] A. Rogerson, J. Nucl. Mater. 159 (1988) 43.
[25] A.T. Motta, R.A. Holt, U. Colak, in: J. Wagemans, M.A. Abderrahim and P. D'hondt (Eds.), Proceedings of the 11th International Symposium on Reactor Dosimetry, In-reactor Dosimetry in the 21st Century, World Scientific, New Jersey (2003) 278.